E JOURNAL

Investigation of the vector length as an influencing variable on the chemical composition in powder bed-based fusion of metals using a laser beam

Nele Kretzer (M. Sc.) [a], Nick Hantke (M. Sc) [a], Dr.-Ing. Tobias Grimm[a],
Prof. Dr.-Ing. Jan T. Sehrt[a]
[a] Ruhr-Universität Bochum Universitätsstraße 150, Bochum, Deutschland

https://doi.org/10.58134/fh-aachen-rte_2024_003

Zusammenfassung Das pulverbettbasierte Schmelzen von Metall mittels Laserstrahl (PBF-LB/M nach DIN EN ISO/ASTM 52900) ist ein etabliertes additives Fertigungsverfahren zur direkten Herstellung von metallischen Bauteilen. Dieses Verfahren unterliegt Einflussgrößen, die die Eigenschaften des hergestellten Bauteils maßgeblich beeinflussen. Scangeschwindigkeit, Laserleistung und Hatchabstand sind entscheidend für die Erzeugung von Schmelzspuren, die zu einer ausreichenden Benetzung und einem dichten Bauteil führen. Um ein geeignetes Parameterfenster zu ermitteln, werden Proben aus AlSi10Mg mit einer definierten Vektorlänge hergestellt und in Qualifizierungsprozessen bewertet. In diesem Beitrag wird der Einfluss der Vektorlänge auf die Bauteileigenschaften, wie Härte, Dichte und chemische Zusammensetzung, untersucht. Es stellt sich die Frage, ob qualifizierte Vektorlängen ohne weitere Untersuchungen und ohne Beeinträchtigung der Bauteilqualität auf beliebige Längen skaliert werden können. Mit Hilfe der energiedispersiven Röntgenfluoreszenzanalyse (EDXRF) und der energiedispersiven Röntgenspektroskopie (EDX) konnte eine Konzentrationsschwankung für das Element Aluminium nachgewiesen werden. Die Proben zeigen eine Veränderung der chemischen Zusammensetzung in Abhängigkeit von der Vektorlänge, die mit EDXRF nachgewiesen wurde. Eine Korrelation zwischen der lokal entlang der Vektorlänge aufgelösten chemischen Veränderung kann jedoch noch nicht festgestellt werden.

Abstract Powder bed fusion of metals using a laser beam (PBF-LB/M according to DIN EN ISO/ASTM 52900) is an established additive manufacturing process for the direct production of metallic components. This process is subject to influencing variables which significantly affect the properties of the manufactured component. Scanning speed, laser power and hatch distance are decisive for the production of melt tracks that result in sufficient wetting and a dense component. In order to determine a suitable parameter window, samples made of AlSi10Mg with a defined vector length are manufactured and evaluated in qualification processes. This article examines the influence of the vector length on the component properties, such as hardness, density and chemical composition. The question arises as to whether qualified vector lengths can be scaled to any length without further investigation and without impairing the component quality. With the help of energy-dispersive X-ray fluorescence analysis (EDXRF) and energy-dispersive X-ray spectroscopy (EDX), it was possible to detect a fluctuation in concentration for the element aluminum. The samples show a change in chemical composition depending on the vector length, detected with EDXRF. However, a correlation between the chemical change resolved locally along the vector length cannot be determined yet.

Introduction

In additive manufacturing, powder bed fusion of metals using a laser beam (PBF-LB/M) [1] has proven to be a powerful tool for the production of complex and functional three-dimensional metal components with precise control over microstructure and mechanical properties [2, 3]. The manufacturing process is based on the principle of layered and selective melting of metallic powder materials in a powder bed. In addition to advantages such as design freedom and the cost-efficient production of unique solutions, PBF-LB/M also faces challenges [4]. The process is subject to various factors that influence the quality of the manufactured components significantly. Influencing variables such as laser power, hatch distance and scanning speed are investigated to qualify process parameters [5, 6] Choosing the right scanning strategy is also essential for successfully producing the selected material's component geometry. Innovative scanning strategies such as constant scan vector times and dynamic power changes within a scan vector offer new possibilities for addressing problems such as distortion formation and residual stresses, e.g., in overhang [7].

The combination of these parameters makes it possible to process metallic materials according to specified criteria to meet the requirements for component quality [8]. In addition to the conditions already summarized in the guidelines, other influences determine the outcome of the build processes [8]. In previous works, the authors have already demonstrated the effect of the chemical composition in powder bed fusion of metals using an electron beam (PBF-EB/M) [9, 10]. The volatilization of light elements in the manufacturing process poses a challenge, as the loss of elements significantly influences for example the mechanical properties of the manufactured component [11].

At this point, the authors address the question of the extent to which a change in the chemical composition is already noticeable in the parameter qualification. Process parameters are usually qualified on cubic-shaped samples and thus on a fixed vector length. Components that are manufactured based on this vector length have not yet been examined for a possible change in chemical composition. Influences caused by the vector length have already been identified in the past [12–16]. Mugwagwa et al. [16] studied the effect of scan vector length on residual stresses in PBF-LB/M of tool steel. Gokcekaya et al. have investigated the influence of vector length on the densification and crystallographic microstructure formation of pure chromium [18]. Another example is the study by Serrano-Munoz et al., which deals with process-related changes in the microstructure of IN718 as a function of vector length [19]. Chemical composition is an important factor in quality assurance, but it is not yet part of the state of the art in additive manufacturing. The hypothesis of this study involves examining the influence both along a scan vector and between scan vectors depending on vector length on possible changes in chemical composition.

Alloys containing light elements with a high vapor pressure are particularly at risk. AlSi10Mg is used as powder feedstock in this study. AlSi10Mg has a high specific strength and is therefore used in industries where weight reduction is crucial, such as aerospace and automotive [20, 21]. AlSi10Mg contains volatile elements such as aluminum and magnesium as the main alloying elements, which can evaporate from the locally scalded melt pools [11, 22].

Material and Methods

Powder characterization

To characterize the starting material, the particle morphology is analyzed using a scanning electron microscope (SEM) (Gemini 2, Carl Zeiss AG). The particle size distribution (Camsizer X2, Microtrac) is determined with a dispersion pressure of 200 kPa.

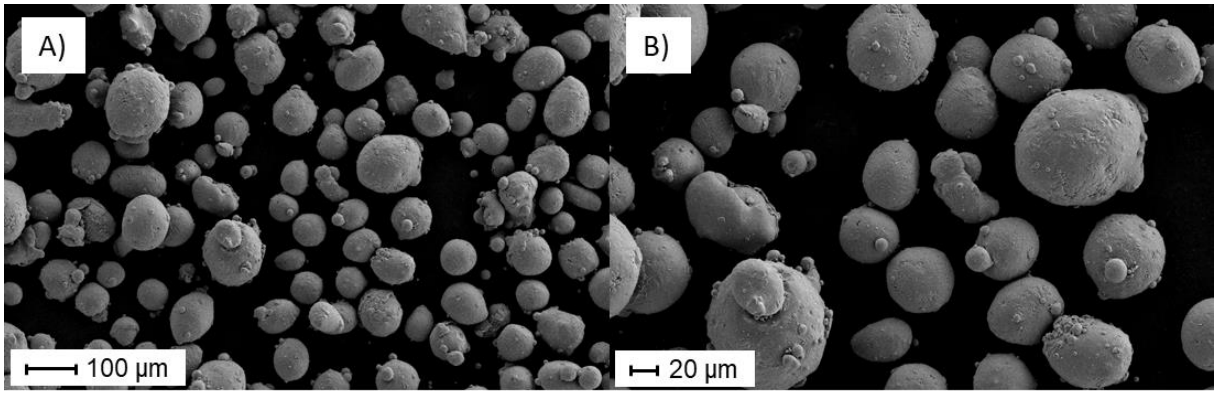

Figure 1: A) Particle morphology of the AlSi10Mg powder (100x magnification), B) Detailed image (250x magnification)

Density and hardness measurement

Three cross-sections of the PBF-LB/M samples are prepared for density measurement, hardness testing, and SEM investigations by grinding and polishing (Saphir 250 A2-ECO, ATM Qness GmbH). The density is determined by the binarization of microscope images (VHX-6000, Keyence). The hardness HV1 of the samples is determined based on five measurements (measured evenly in the center over the length of the sample) of a cross-section using the hardness tester ZHV3 (ZwickRoell). According to the recommendation of VDI Guideline 3405 Part 2 [8, 23], the average hardness is determined without considering the hardest and the softest indentation. For samples 3 and 6, only three hardness indentations can be made due to the small cross-section. The average hardness values for these samples is determined from the three indentations.

Measurement of chemical composition

Energy-dispersive X-ray fluorescence analysis (EDXRF) (Vanta C series, Olympus) determines the chemical composition of the starting powder and the bulk samples. The starting material and the solid samples are measured in a cuvette through a thin film foil. A silicon drift chamber detector detects the photons in the X-ray fluorescence radiation of the sample. The result is a pulse height spectrum that reflects the number of photons at a specific energy. The evaluation method is database-based [24] and uses mass values of the elements. Energy dispersive X-ray spectroscopy (EDX) (Gemini 2, Carl Zeiss AG) is used to determine the local element distribution. In preparation for the measurement, the samples were embedded in a conductive embedding compound and ground on the top surface. As some of the samples were very long, it was not possible to carry out the usual line scans. For this reason, individual EDX-mappings are carried out and evaluated over the sample length. At this point, it must also be mentioned that the embedding material created measurement noise, which is reflected in the results by a lower measured aluminum value.

Feedstock material

Gas-atomized AlSi10Mg powder (m4p material solutions GmbH) is used for the study. The chemical composition of the powder material was determined using EDXRF (Table 1).

Table 1: Chemical composition of initial powder AlSi10Mg

	Al	Si	Fe	Mn	Mg
%	88.52	10.445	0.18	0.01	0.67
+-3σ	0.08	0.07	< 0.01	< 0.01	0.03

The particle size distribution is measured using the principle of dynamic image analysis (Fig. 2). The powder material has a gaussian-like particle size distribution with a trimodal shape (q3). The three maxima appear in the right thigh of the curve at approx. 32 µm, 45 µm and 50 µm. The particle size distribution has a fine fraction (< 20 µm, left thigh) and a coarser fraction (> 60 µm, right thigh). The percentiles can be read from the cumulative curve Q3 (D10 (25.42 µm), D50 (36.87 µm) and D90 (52.4 µm)). The powder has a typical range for the PBF-LB/M application. The particle morphology is qualitatively analyzed using scanning electron microscope images (Zeiss AG) (Fig. 1). The particles have a rough surface with some satellite adhesions.

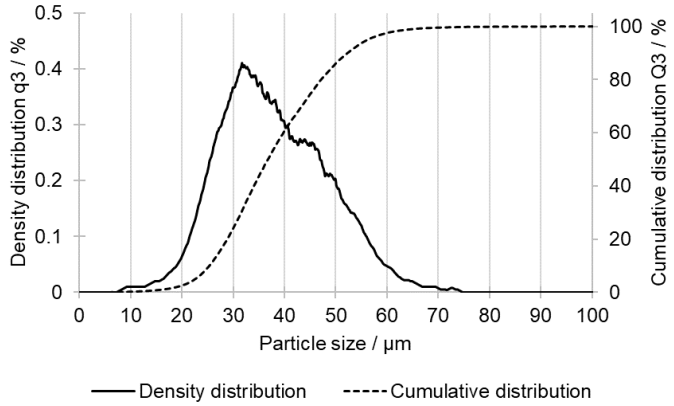

Figure 2: Measured values for particle size distribution

The general shape of the particles tends to be spherical. Elongated particles can also be detected in the sample, harming the powder spreadability. A detailed image is shown in Fig. 1 B).

PBF-LB/M process

The PBF-LB/M samples are produced on the AconityMIDI PBF-LB/M system (Aconity3D GmbH). The energy source is a 400 W fiber laser with a wavelength of 1070 nm and variable focus diameter, operated with a diameter of 80 µm for the test series. For this study, nine rectangular samples with a fixed width of 5 mm and a variable length (1.25, 2.5, 5, 10, 15, 20, 25, 30 and 35 mm) were prepared, as shown in Figure 3 A).

The build process takes place under an argon-inert gas atmosphere. The following parameters are used: 220 W Laser power, 1800 mm · s^{-1} scan velocity, 30 µm layer

thickness. The build job setup is depicted in Figure 3 A), and the hatch orientation is shown in Figure 3 B). To keep the vector length constant, a hatch rotation of 180° in between

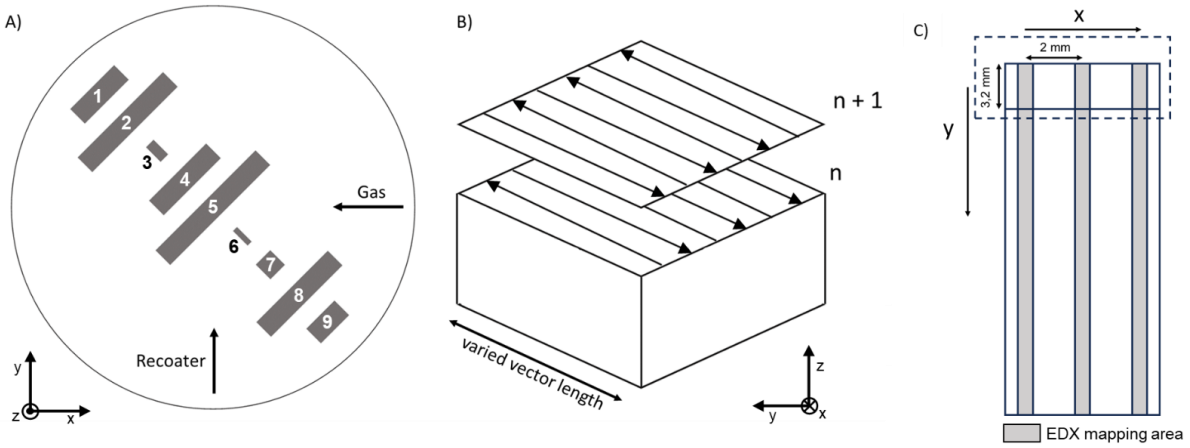

Figure 3: Representation A) of the sample orientation in the construction space B) of the hatch rotation by 180° and C) diagram of the measuring grid of the EDX analysis based on a schematic sample

layers is chosen.

Results and discussion

Density and hardness

Figure 5 A) shows the relative density of the samples plotted against their vector lengths. All samples produced have a relative density of > 99.5 %. The relative density tends to decrease with increasing vector lengths. The process parameters used were determined in a preliminary study using cube-shaped samples with an edge length of 5 mm. The fact that the highest relative density of 99.84 % is achieved for samples with a vector length of 5 mm and that the density decreases with increasing vector lengths shows that the determined process parameters cannot be transferred to longer vector lengths without re-qualification. The longer the vector, the longer the time it takes for the laser to return to the same point when the next vector is exposed. It is assumed that this causes more heat to be dissipated from the previously exposed vector and the already exposed layer due to thermal conduction, which means that more energy is required to achieve dense samples [8]. In Figure 5 B) the hardness of all samples produced in HV1 with its standard deviation is shown. The hardness values vary between 120 and 140 HV1, which is typical for the material [24]. The hardness for the longer samples is slightly increased, but there is no correlation between the values of relative density and hardness. A change in hardness cannot be attributed to the loss of aluminum either, as magnesium and silicon are responsible for the strength and hardness of the material [26, 27].

In general, the comparatively high standard deviations stand out for samples under 5 mm in length and from 25 mm in length. In the case of the short samples, this may be due to the smaller sample area and the lower number of measurements carried out, while in the case of samples 25 mm and longer, a higher number of pores may be the reason for a higher standard deviation.

EDXRF-Analysis

The samples are measured in the as-built condition on the top surface and on a filed side surface using the EDXRF. The concentration of the alloying elements aluminum and silicon are shown in Figure 4. The course of the graphs shows a trend that correlates with the vector length of the samples, both on the top and side surfaces. As the vector lengths increase, there is also a slight increase in the relative aluminum concentration from 90.5 to approx. 91 wt.%. Analogous to the increase in the aluminum concentration, a decrease

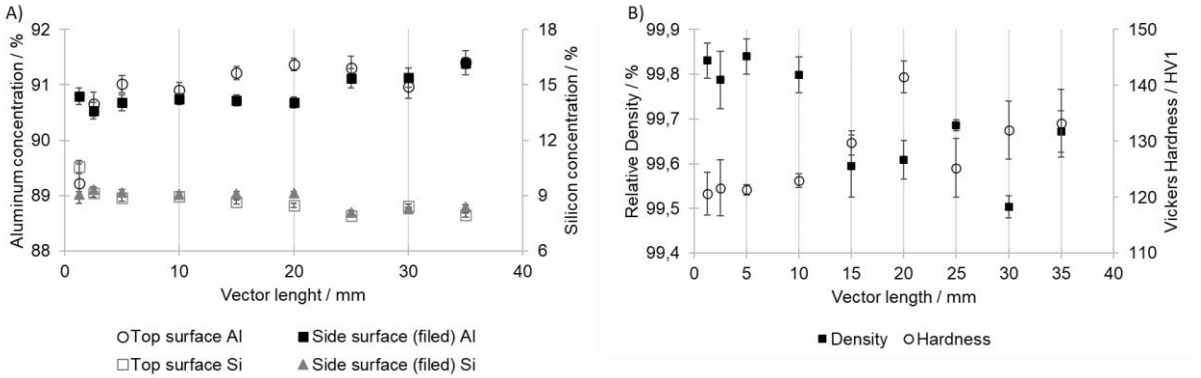

Figure 4: Change in relative elemental concentration of A) Aluminum and Silicon (EDXRF) and B) Relative density and Hardness as a function of the vector length

in the relative silicon content can be observed, from 9.2 to approx. 8.5 wt.-%. At the same time, a difference in the measured areas cannot be determined.

EDXRF-Analysis

The EDX analysis is carried out in addition to the examination with the EDXRF to determine the chemical composition locally at specified measuring points in a grid-like arrangement. A representation of the measured grid can be found in Figure 3 C), in which the gray stripes indicate the area covered by the EDX mapping. The changes in the element concentration over the length of the sample (vertical, y-direction) and the width of the sample (horizontal, x-direction) are now considered. To establish a comparison, the range of variation of the element concentration is determined for both orientations. This range results from the respective minima and maxima of the measured element concentration. The results are shown in Fig. 5.

The average values of the aluminum concentration (Fig. 5 A) shown for the range of variation in the y-direction (0.78) are, on average, comparatively higher than those of the range of variation in the x-direction (1.21). The t-test results nevertheless show that these differences are not statistically significant at a conventional level ($p=0.188$). A change in the element concentration is nevertheless measurable. The results of the silicon concentration (Fig. 5 B) show more clearly that a change in the vector length has no significant influence on the element concentration. There is no detectable statistical difference between changes in the vertical sample and the horizontal sample ($p=0.792$). The average values of the variation margins in the x-direction (0.19) and y-direction (0.18) are also lower than the values for aluminum on the one hand and do not differ noticeably on the other. The variation ranges of magnesium and iron (Fig. 5 C and D) are, on average, below 0.1 % and thus show an extremely low fluctuation of the element concentration over the vector length in the x- and y-direction. The t-test also indicates that the differences

between the ranges for magnesium (p=0.118) and iron (p=0.397) are not statistically significant.

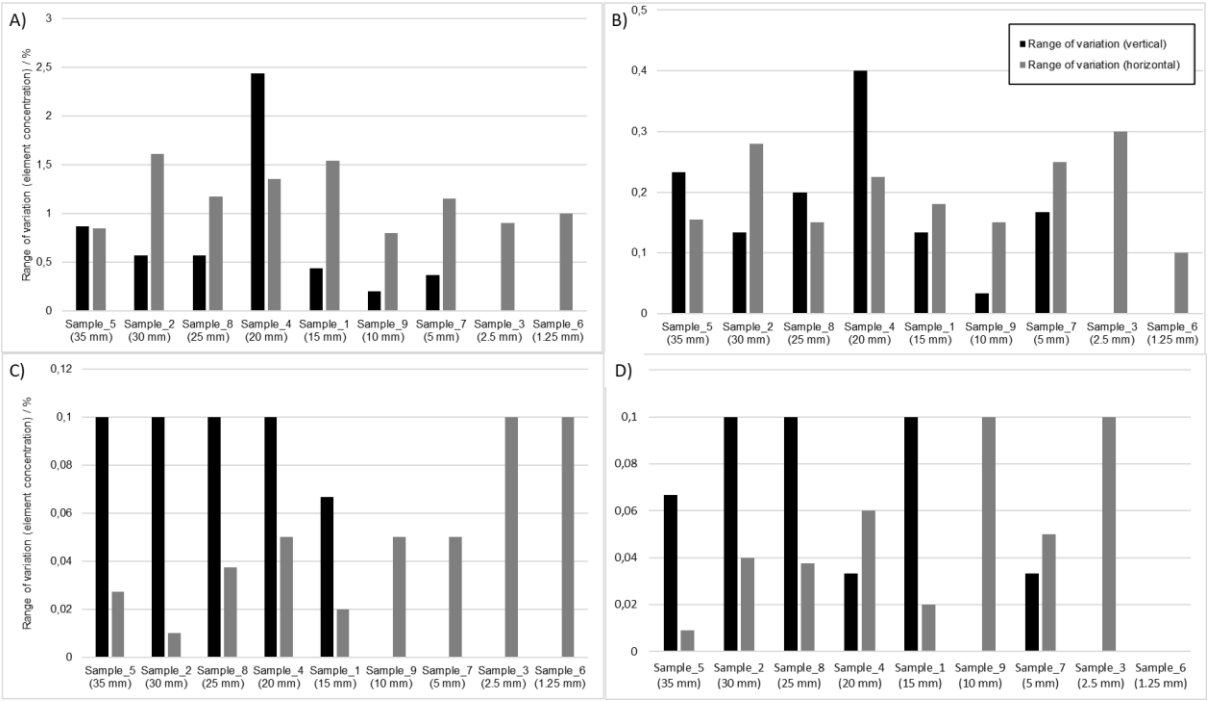

Figure 5: Range of variation for the elements A) aluminum, B) magnesium, C) silicon and D) iron

What is nevertheless noticeable for the variation ranges of the aluminum and silicon concentration (Fig 5 A) and B)) is that the highest fluctuation of the element concentration in both cases is at sample 4 (20 mm). This sample already stood out because of the higher measured value in the hardness test.

There are studies on the influence of the temperature distribution on the development of residual stresses and distortion in the PBF-LB/M process [16, 22, 27]. No information on the phenomenon described above can be found in the literature. This interesting result requires further investigation. For this reason, further work is currently underway to explain the origin of this phenomenon at the present time.

Conclusion and outlook

Only the results for the aluminum concentration show a slight change in the material composition over the entire sample surface, which correlates with the vector length.

However, this finding cannot be confirmed in y-direction along the vector by local elemental analysis using EDX. The results show no significant change in the element concentration along the vector. Fluctuations can only be detected in samples 4 and 5 but do not indicate a correlation between the investigated variables. Looking at the values transverse to the vector direction also shows no significant change in the chemical composition. A fluctuation in concentration can only be measured for the element aluminum. A statistically significant relationship could not be found for the elements examined. From this, there is no connection between looking at the element change in the x and y directions. However, the shift in aluminum concentration, which could be detected for both orientations, remains intriguing.

Further investigations are necessary to get a better understanding of the phenomenon, for example the examination of the microstructure in order to obtain further important information about the characteristics of the component properties.

Acknowledgment

This Project is supported by the Federal Ministry for Economic Affairs and Climate Action (BMWK) on the basis of a decision by the German Bundestag. Funded by the Deutsche Forschungsgemeinschaft (DFG, German Research Foundation) – 410107213. Furthermore, the authors express their sincere thanks to the DFG for funding the major research instrumentation 426714238.

Contact details

Nele Kretzer (corresponding author)
Universitätsstraße 150, 44801 Bochum
E-Mail: nele.kretzer@ruhr-uni-bochum.de
WEB: https://www.ham.ruhr-uni-bochum.de/

References

[1] Additive Fertigung- Grundlagen-Terminologie, DIN EN ISO/ASTM 52900:2022-03, Berlin.

[2] J. P. Oliveira, A. D. LaLonde und J. Ma, "Processing parameters in laser powder bed fusion metal additive manufacturing," Materials & Design, Jg. 193, S. 108762, 2020, doi: 10.1016/j.matdes.2020.108762.

[3] S. Sanchez et al., "Powder Bed Fusion of nickel-based superalloys: A review," International Journal of Machine Tools and Manufacture, Jg. 165, S. 103729, 2021, doi: 10.1016/j.ijmachtools.2021.103729.

[4] H. Ali, H. Ghadbeigi und K. Mumtaz, "Effect of scanning strategies on residual stress and mechanical properties of Selective Laser Melted Ti6Al4V," Materials Science and Engineering: A, Jg. 712, S. 175–187, 2018, doi: 10.1016/j.msea.2017.11.103.

[5] M. Schmitt, B. Kempter, G. Schlick und G. Reinhart, "Parameter identification approach for support structures in laser powder bed fusion and analysis of influencing factors," Procedia CIRP, Jg. 94, S. 260–265, 2020, doi: 10.1016/j.procir.2020.09.049.

[6] A. Leis, R. Weber und T. Graf, "Process Window for Highly Efficient Laser-Based Powder Bed Fusion of AlSi10Mg with Reduced Pore Formation," Materials (Basel, Switzerland), Early Access. doi: 10.3390/ma14185255.

[7] H. Jia, H. Sun, H. Wang, Y. Wu und H. Wang, "Scanning strategy in selective laser melting (SLM): a review," Int J Adv Manuf Technol, Jg. 113, 9-10, S. 2413–2435, 2021, doi: 10.1007/s00170-021-06810-3.

[8] Additive Fertigungsverfahren - Grundlagen, Begriffe, Verfahrensbeschreibungen, 3405:2014-12, Verein Deutscher Ingenieure e.V.

[9] N. Kretzer, R. Ortmann, T. Grimm und J. T. Sehrt, Hg., Untersuchungen zum Einfluss der Energiequelle auf die Oberflächenqualität und die chemische Zusammensetzung in der pulverbettbasierten additiven Fertigung (Deutscher Verband für Materialforschung und –prüfung e.V), 2023, doi: 10.48447/WP-2023-255.

[10] N. Kretzer, R. Ortmann, T. Grimm und J. T. Sehrt, "Einfluss von Prozessparametern auf die chemische Zusammensetzung von AlSi10Mg-Bauteilen beim pulverbettbasierten Elektronen-Strahlschmelzen," in Werkstoffe und Bauteile auf dem Prüfstand, Zimmermann, M., Ed., Hg. (Deutscher Verband für Materialforschung und -prüfung e.V), 2023.

[11] M. Bärtl, X. Xiao, J. Brillo und F. Palm, "Influence of Surface Tension and Evaporation on Melt Dynamics of Aluminum Alloys for Laser Powder Bed Fusion," J. of Materi Eng and Perform, Jg. 31, Nr. 8, S. 6221–6233, 2022, doi: 10.1007/s11665-022-06592-z.

[12] S. Greiner und D. Drummer, "Understanding aspect ratio effects in Laser Powder Bed Fusion of polyamide 12 by means of infrared thermal imaging," Procedia CIRP, Jg. 111, S. 253–256, 2022, doi: 10.1016/j.procir.2022.08.060.

[13] L. Englert, V. Schulze und S. Dietrich, "Concentric Scanning Strategies for Laser Powder Bed Fusion: Porosity Distribution in Practical Geometries," Materials (Basel, Switzerland), Early Access. doi: 10.3390/ma15031105.

[14] F. Schmeiser, E. Krohmer, N. Schell, E. Uhlmann und W. Reimers, "Internal Stress Evolution and Subsurface Phase Transformation in Titanium Parts Manufactured by Laser Powder Bed Fusion—An In Situ X-Ray Diffraction Study," Adv Eng Mater, Jg. 23, Nr. 11, 2021, Art. Nr. 2001502, doi: 10.1002/adem.202001502.

[15] S. Chowdhury et al., "Laser powder bed fusion: a state-of-the-art review of the technology, materials, properties & defects, and numerical modelling," Journal of Materials Research and Technology, Jg. 20, S. 2109–2172, 2022, doi: 10.1016/j.jmrt.2022.07.121.

[16] L. Li, H. Chen, X. Wang und Z. Liao, "Effects of vector length on the melt pool morphology and grain structure characteristics of Alloy 718 in laser powder bed fusion," Journal of Materials Processing Technology, Jg. 326, S. 118317, 2024, doi: 10.1016/j.jmatprotec.2024.118317.

[17] L. Mugwagwa, D. Dimitrov, S. Matope und I. Yadroitsev, "INVESTIGATION OF THE EFFECT OF SCAN VECTOR LENGTH ON RESIDUAL STRESSES IN SELECTIVE LASER MELTING OF MARAGING STEEL 300," SAJIE, Jg. 30, Nr. 4, 2019, doi: 10.7166/30-4-2096.

[18] O. Gokcekaya et al., "Effect of Scan Length on Densification and Crystallographic Texture Formation of Pure Chromium Fabricated by Laser Powder Bed Fusion," Crystals, Jg. 11, Nr. 1, S. 9, 2021, doi: 10.3390/cryst11010009.

[19] I. Serrano-Munoz et al., "High-resolution Bragg-edge neutron radiography detects grain morphology in PBF-LB/M IN718," Materialia, Jg. 30, S. 101827, 2023, doi: 10.1016/j.mtla.2023.101827.

[20] D. Dai und D. Gu, "Effect of metal vaporization behavior on keyhole-mode surface morphology of selective laser melted composites using different protective atmospheres," Applied Surface Science, Jg. 355, S. 310–319, 2015, doi: 10.1016/j.apsusc.2015.07.044.

[21] H. Qin, V. Fallah, Q. Dong, M. Brochu, M. R. Daymond und M. Gallerneault, "Solidification pattern, microstructure and texture development in Laser Powder Bed Fusion (LPBF) of Al10SiMg alloy," Materials Characterization, Jg. 145, S. 29–38, 2018, doi: 10.1016/j.matchar.2018.08.025.

[22] J. Yin et al., "Vaporization of alloying elements and explosion behavior during laser powder bed fusion of Cu–10Zn alloy," International Journal of Machine Tools and Manufacture, Jg. 161, S. 103686, 2021, doi: 10.1016/j.ijmachtools.2020.103686.

[23] L. Parry, I. A. Ashcroft und R. D. Wildman, "Understanding the effect of laser scan strategy on residual stress in selective laser melting through thermo-mechanical simulation," Additive Manufacturing, Jg. 12, S. 1–15, 2016, doi: 10.1016/j.addma.2016.05.014.

[24] DIN EN 10027-2:2015-07, Bezeichnungssysteme für Stähle_- Teil_2: Nummernsystem; Deutsche Fassung EN_10027-2:2015, Berlin.

[25] H. Hyer et al., "Understanding the Laser Powder Bed Fusion of AlSi10Mg Alloy," Metallogr. Microstruct. Anal., Jg. 9, Nr. 4, S. 484–502, 2020, doi: 10.1007/s13632-020-00659-w.

[26] M. M. Collur, A. Paul und T. Debroy, "Mechanism of alloying element vaporization during laser welding," Metall Trans B, Jg. 18, Nr. 4, S. 733–740, 1987, doi: 10.1007/BF02672891.

[27] H. Zhao und T. Debroy, "Weld metal composition change during conduction mode laser welding of aluminum alloy 5182," Metall Mater Trans B, Jg. 32, Nr. 1, S. 163–172, 2001, doi: 10.1007/s11663-001-0018-6.

[28] K. S. Ramani, C. He, Y.-L. Tsai und C. E. Okwudire, "SmartScan: An intelligent scanning approach for uniform thermal distribution, reduced residual stresses and deformations in PBF additive manufacturing," Additive Manufacturing, Jg. 52, S. 102643, 2022, doi: 10.1016/j.addma.2022.102643.